



HAL
open science

Impact cratering rate consistency test from ages of layered ejecta on Mars

Anthony Lagain, Sylvain Bouley, David Baratoux, F. Costard, Mark Wieczorek

► **To cite this version:**

Anthony Lagain, Sylvain Bouley, David Baratoux, F. Costard, Mark Wieczorek. Impact cratering rate consistency test from ages of layered ejecta on Mars. *Planetary and Space Science*, 2020, 180, pp.104755. 10.1016/j.pss.2019.104755 . hal-02459037

HAL Id: hal-02459037

<https://hal.science/hal-02459037>

Submitted on 4 Dec 2020

HAL is a multi-disciplinary open access archive for the deposit and dissemination of scientific research documents, whether they are published or not. The documents may come from teaching and research institutions in France or abroad, or from public or private research centers.

L'archive ouverte pluridisciplinaire **HAL**, est destinée au dépôt et à la diffusion de documents scientifiques de niveau recherche, publiés ou non, émanant des établissements d'enseignement et de recherche français ou étrangers, des laboratoires publics ou privés.

Impact cratering rate consistency test from ages of layered ejecta on Mars.

Anthony Lagain^{1,2*}, Sylvain Bouley^{1,3}, David Baratoux⁴, François Costard¹ and Mark Wieczorek⁵

¹GEOPS-Géosciences Paris Sud, Université Paris-Sud, CNRS, Université Paris-Saclay, Rue du Belvédère, Bâtiment 504-509, 91405 Orsay, France.

²School of Earth and Planetary Science, Curtin University, GPO Box U1987, Perth, WA, 6845, Australia.

³Institut de Mécanique Céleste et de Calcul des Ephémérides, UMR8028, 77 avenue Denfert-Rochereau, 75014 Paris, France.

⁴Geosciences Environnement Toulouse, Université de Toulouse III UMR 5563, 14 Avenue Edouard Belin, 31400 Toulouse, France.

⁵Université Côte d'Azur, Observatoire de la Côte d'Azur, CNRS, Laboratoire Lagrange, Nice, France

*Corresponding author: Anthony Lagain (anthony.lagain@gmail.com)

Key Words: Impact craters ; Mars ; Impact rate ; Layered ejecta craters

Key Points:

- We have produced a complete set of large (>5 km in diameter) impact crater ages formed over Acidalia Planitia (Mars) using the population of small impact craters (>200 m in diameter) on their ejecta, and a constant impact rate and production function.
- The impact rate inferred from this set of ages is inconsistent with the assumption of a constant production function and impact rate.
- We interpret this inconsistency as a result of variations in the size-frequency distribution of large impactors in the main belt over the past 2 Ga, probably caused by asteroid break-ups within the main belt.

29 **Abstract**

30 Ages of geological units of planetary bodies are determined from impact crater counts on their
31 surface. These ages are model-dependent, and several models largely used in the community
32 assume a constant production function and a constant cratering rate over the last 3 Ga. We have
33 mapped the population of small impact craters (> 200 m in diameter) formed over a population of
34 large impact craters (>5 km in diameter) with layered ejecta on Acidalia Planitia, Mars. We have
35 deduced the age of each large impact crater under the assumption of a constant impact rate and
36 constant production function. The impact rate inferred from this set of ages is, however, not
37 constant and show a significant increasing during the last ~1 Ga compared to chronology models
38 commonly used. We interpret this inconsistency as an evidence for temporal variations in the size-
39 frequency distribution (SFD) of impactors in the main belt, consistent with recent studies argued
40 for a late increasing of the large impactor flux on Earth and the Moon.

41 **1 Introduction**

42 The collisional history in the inner Solar System since planetesimal formation has received
43 considerable attention as the geological histories of all terrestrial planets and the Moon are inferred
44 from impact crater counts (Bottke, W. et al., 2000 ; Neukum et al., 2001 ; Le Feuvre and
45 Wieczorek, 2011). Radiometric crystallization ages of Apollo samples suggest a decrease of the
46 cratering rate around ~3.9 to ~3.5 Ga, followed by a constant rate after 3 Ga for kilometer-sized
47 craters (Stöffler et al., 2006). Craters counts are interpreted based on this general pattern with
48 variations among authors regarding the details of the mathematical expression of the impact crater
49 production function (PF).

50 Recent studies such as Hartmann et al.(2010) demonstrate that the impact crater production
51 function for deca-meter scale craters is consistent with the chronology system used to date young
52 geological features on Mars. However, a constant post ~3.0 Ga impact rate and steady PF is only
53 weakly supported with insufficient constraints for ages younger than 3.5 Ga. In particular, there
54 are no Apollo sample with an age between 3.25 and 0.8 Ga, and only 5 samples younger than 0.8
55 Ga (Stöffler et al., 2006 , Tikoo et al., 2017). This paradigm has also been challenged by the
56 apparent increase of landslide activity as function of time at Valles Marineris, Mars, a paradox
57 which could be resolved with a progressive decline by a factor of 3 of the cratering rate over the
58 last 3 Ga (Quantin et al., 2007). There are also pieces of evidence for one or two major cratering
59 spikes over the last 500 Ma due to asteroid breakup(s) in the main asteroid belt (Culler et al., 2000
60 ; Zellner and Delano, 2015 ; Bottke et al., 2007 ; Nesvorny et al., 2002 ; Quantin et al., 2015). The
61 recent variation of the impact cratering rate has been quantified on the Moon using the
62 thermophysical characteristics of lunar impact ejecta (Mazrouei et al. 2019). That study showed
63 that the rate of formation of impact craters on our satellite has been two to three times higher over
64 the last 290 Ma than it had been over the previous 700 Ma. These fluctuations could also explain
65 the apparent deficit of large craters on Earth between ~300 and 650 Ma, which was previously
66 considered to reflect a preservation bias (Mazrouei et al. 2019).

67 Here we propose a new test of the validity of the assumed constant impact rate and steady
68 state SFD of impactors over the last 3 billion years on Mars. The applicability of this test depends
69 on the existence of a region of Mars with a population of several tens of large impact craters (>5
70 km diameter) for which ages could be inferred from the population of small craters (> 200 m) that
71 overprinted their ejecta. Hereafter, the expression “large crater(s)” will refer to impact craters
72 larger than 5 km in diameter, whereas the expression “small crater(s)” will refer to the population

73 of impact craters with diameters ranging typically between 200 m and 1 km that were used to date
74 the formation of the large impact craters. This region should not be affected significantly by
75 resurfacing processes, at least down to the scale of the small impact craters used to date each large
76 crater. The ages of large impact craters are determined using a constant impact rate and a constant
77 PF over time (Hartmann, 2005). This set of ages is then used to describe the rate at which the large
78 impact craters formed. If the PF was indeed constant, then the impact rate determined from the
79 ages of the large craters should be constant as well. Our self-consistency test has the aim to detect
80 potential temporal variations in the crater size-frequency distribution. Any variation of the inferred
81 impact rate would therefore indicate that the initial assumption concerning a steady state of the
82 production function is not valid. We chose to apply this test to a population of impact craters with
83 continuous layered ejecta blankets. This type of ejecta morphology is particularly amenable to
84 crater counting using small impact craters down to 100 m in diameter (Baratoux et al., 2007 ;
85 Kadish and Head, 2014).

86 Following this introduction, the method section describes the approach for dating layered
87 ejecta deposits, the selection criteria to identify a region of Mars comprising a suitable population
88 of craters with layered ejecta, and the calculation of the impact rate inferred from the population
89 of large craters. The crater counts and the inferred formation rate of large impact craters as a
90 function of time are described in the following section. Implications of the test results for the
91 validity of the constant impact rate and steady state size-frequency distribution of impactors in the
92 main belt are discussed in the last section.

93 **2 Methods and selection of the study area**

94 **2.1 Dating layered ejecta impact craters**

95 Some of the Martian impact craters larger than 5 km in diameter exhibit continuous layered
96 ejecta deposits. These ejecta deposits offer a better and larger area for the counting of small
97 superposed craters in comparison to the more common ballistic ejecta deposits and/or rayed craters
98 (Baratoux et al., 2007 ; Quantin et al., 2015). However, erosion processes can obliterate impact
99 craters superposed on ejecta blankets. Self-secondaries are also common on the ejecta of Martian
100 impact craters. Whereas background secondaries are indistinguishable from the primary
101 population and should be take into account for a surface age dating (Hartmann, 2005), clusters of
102 secondary craters need to be excluded from crater counts.

103 Layered ejecta morphologies are complex and do not necessarily exhibit a homogeneous
104 density of impact craters. In order to identify those regions of the ejecta layer(s) where the crater
105 population is the most representative of the ejecta blanket emplacement age, we have mapped in
106 detail the Arandas crater ejecta blanket. This 24.8 km impact crater, located at 15.17°W and
107 42.77°N, exhibits two well-preserved ejecta layers and is classified as “Double Layered Ejecta
108 Rampart Sinuous” according to the scheme of Barlow et al. (2000). The map of the impact structure
109 and its ejecta blankets is based on Context Camera (CTX, Mars Reconnaissance Orbiter) imagery,
110 offering a resolution of 6 meters per pixel and on the THERmal EMission Imaging System Daytime
111 IR (THEMIS, Mars Odyssey) data offering a resolution of 100 meters per pixel (Christensen et al.,
112 2004). The size-distribution of craters larger than 200 m in diameter is measured using the
113 CraterTools module for the ArcGIS software (Kneissl et al., 2011) over the entire ejecta blanket
114 and ages are estimated based on the approach of Hartmann (2005) that assumes a constant PF and
115 impact rate.

116 From the center of the crater to its rim, the geological map of Arandas (Figure 1a) is divided
117 into four morphological units: the central peak (Cp), the slumped central peak material (Scpm),
118 the crater floor (F) and the exposed wall rock (Ewr). The inner and outer ejecta layers may be sub-
119 divided into sub geological units. The inner layer extends between 1.1 and 3 crater radii (R_c). A
120 hummocky, smooth and non-striated unit (He, Figure 1b) adjacent to the crater rim is identified on
121 the inner ejecta layer. It extends to approximately 2 kilometers away from the crater rim. Adjacent
122 to the He unit, the inner layer unit also exhibits radial ridges and a relatively smooth surface (Figure
123 1c). Outward is found a unit with radial grooves and ridges (Sil, Figure 1d). The most external unit
124 of the inner layer, named “the chaotic inner layer” (Cil), exhibits concentric crests, with chaotic
125 morphologies, including pseudo-circular depressions and hummocky features with radial ridges
126 progressively vanishing (Figure 1e). The external edge of this unit is characterized by a terminal
127 rampart, which is a common feature for layered ejecta deposits. The outer layer (Ol) exhibits a
128 lobate morphology (Figure 1f) and extends to 4-8.2 R_c . Some lobes show a thickened, distal
129 rampart (DI) (Figure 1g). Our mapping of impact craters included all craters larger than 200 m in
130 diameter on the layered ejecta blankets.

131 Qualitatively, four areas, belonging to the Ol unit, present an excess of impact craters in
132 comparison with the rest of the ejecta deposit (red ellipses on Figure 1a named “overcratered
133 areas”). Furthermore, the inner layer has fewer impact craters than the outer layer (Figure 1),
134 suggesting that the outer layer could include a larger number of secondaries and/or the inner layer
135 was modified by post-impact processes (Weiss and Head, 2013). Such processes include mass
136 wasting processes related to the presence of sub-surface ice. We have therefore excluded the inner
137 layer from our counting and consider the outer layer provided that the larger number of craters is
138 not solely the consequence of secondary craters (Lagain et al., 2015).

139 The crater density on the outer layer is, however, heterogeneous. The heterogeneity is
140 probably due to secondary craters (Zanetti et al., 2017) associated with Arandas itself or with large
141 nearby impact craters. Secondary craters usually do not dominate the entire population of craters
142 for the diameter range that we investigate (Werner et al., 2008). Secondaries are also usually
143 clustered, offering a possibility to distinguish primary craters from secondary craters. We have
144 used the Randomness Analysis Tool (Michael et al., 2012) to help identify and remove from the
145 counting areas regions that were dominated by clusters of secondaries. Several count regions were
146 defined, with the goal of obtaining one or more count regions where the craters were statistically
147 not clustered for at least the 3 largest diameter bins ($\sqrt{2}$ -bins) (top of Figure 2). The data were then
148 fitted with Hartmann's isochrons by a Poisson analysis (Michael et al., 2016) implemented in the
149 CraterStats II software (Michael et al., 2010) (bottom of Figure 2). The μ -notation is used here
150 when it is not immediately clear that the derived age is in fact a model age that depends upon an
151 assumed production function and chronological system (Michael et al., 2016). The analysis that
152 was the least clustered was for the northern part of the outer ejecta layer, which provided a best fit
153 model age of $389 \pm_{58}^{58}$ Ma that we take as the formation age of the crater.

154 One source of error that can potentially bias the interpretation of crater counts is the
155 physical properties of the terrain. Kirchoff et al. (2015) and Dundas et al. (2010) have shown that
156 ages derived from crater counts respectively on the Moon and on Mars can be biased due to the
157 variable properties of the target materials. For instance, the impact of an asteroid of a given size
158 and velocity will produce a crater with different final diameters when the target is composed of
159 consolidated or unconsolidated rocks. This bias may affect the entire impact crater population used
160 for dating by a shift in diameter of the crater size-frequency distribution. This issue would be more
161 important for craters smaller than 1 km in diameter, which are more sensitive to variations of the

162 near-surface physical properties than would be larger impact structures. Significant variations in
163 the target's physical properties between the outer layer of an ejecta deposit, composed of
164 brecciated material, and the surrounding terrains are to be expected. However, Wulf and
165 Kenkmann (2015) have shown that the thickness of the inner ejecta blanket of a Double Layered
166 Ejecta Rampart Sinuous crater of 10 km diameter is typically 50 meters, while the outer layer is
167 thinner, typically a dozen meters. Impact craters larger than a few hundreds of meters in diameter
168 should hence excavate through the entire outer layer ejecta down to the underlying rocks that
169 should represent the dominant fraction of the excavated volume. The final crater diameter may
170 thus be dominated by the physical properties of the underlying rocks. We will therefore neglect
171 possible target property effects of the outer ejecta layer on the crater SFD for craters larger than
172 200 m.

173 The lessons learned from Arandas crater will be applied for the dating of all other layered
174 ejecta impact craters in the study region, which will be defined in the following section. In
175 particular, the counting of all craters larger than 200 m in diameter superposed on the outer ejecta
176 blankets will be performed, and count regions will be refined by using the Random Analysis Tool.
177 By using the Hartmann (2005) chronology system (other chronology systems will also be used to
178 date each crater, see section 3 for more details), an isochron will then be fitted using at least the 3
179 largest diameter bins of the crater SFD.

180 **2.2 Study area selection**

181 Our goal is to find a region of Mars where a complete cratering record for craters larger
182 than 5 km in diameter is recorded. Two criteria should be met for this purpose: (1) all craters
183 belonging to that region and larger than 5 km in diameter must exhibit continuous layered ejecta
184 blankets since ages for other types of ejecta morphologies are not easily obtained, (2) the

185 resurfacing activity of that region should be as low as possible, allowing us to extract a CSFD
186 representative of the crater age and not a crater retention age related to a resurfacing episode
187 (Michael et al., 2010). The regions poleward of 45° latitude must be excluded for this reason since
188 they have been affected by degradation due to climate-related processes such as dust/eolian/ice
189 mantling and freeze/thaw erosion (Schon et al., 2012). Nevertheless, degradation and obliteration
190 of impact craters may also occur at lower latitudes (Kreslavsky and Head, 2002, 2003, 2018). In
191 addition to these criteria, the region should be old and large enough to hold several tens of impact
192 craters to allow the derivation of a statistically reliable impact rate as a function of time.

193 Using the most recent catalogues of impact craters larger than 5 km in diameter (Robbins
194 et al. 2012), we have found only one single area, located at the south of Acidalia Planitia (33° -
195 46° N/ 46° - 10° W) which satisfies the first criteria (Figure 3a and 3b). This region has a surface area
196 of 767 000 km². It comprises 53 impact craters with layered ejecta larger than 5 km in diameter.
197 This region belongs to the largest unit of the northern plains, the Vastitas Borealis Formation
198 (VBF) (Tanaka et al., 2014), which exposes an ~100 m-thick sedimentary deposit resulting from
199 multiple episodes of outflow-channel discharges (Carr and Head, 2010). The cratering density
200 measured on these deposits (Platz et al., 2013, Tanaka et al., 2014) is consistent with an
201 emplacement that occurred during the transition between the Hesperian and the Amazonian
202 periods (~3 Ga).

203 The second selection criteria would be satisfied if the density of small craters were
204 homogeneous over the entire region, with the exception of within the ejecta layers of large impact
205 craters. To determine if this is the case, a global crater density map was computed over Acidalia
206 Planitia for craters larger than 500 m in diameter. The crater density map was obtained by using a
207 square moving window with a size of 20 km over the study area. The size of the window was

208 optimized manually and approximately reflects the maximum distance separating the most isolated
209 crater to its nearest neighbor. The window was moved in steps of 5 km, and to avoid any edge
210 effects, crater densities on the borders of the map include impact craters beyond the map border.
211 An age map (Fig 3.b) was determined from the crater density map by applying the Hartmann's
212 chronology system (Hartmann, 2005). The same methodology was applied to construct another
213 density and age map for craters larger than 250 m for a sub-region of Acidalia Planitia. This sub-
214 region corresponds to the area where the density of craters with diameters greater than 500 m is
215 the highest (Fig. 3c). For this map, the crater density has been determined by using a smaller
216 moving window with a size of 5 km.

217 Limited variations of the impact crater density are observed in the study region plotted in
218 Figure 3b, with most areas falling within the range of model ages of 2.00–2.25 Ga. Lower crater
219 densities (younger ages) are found systematically in the immediate vicinity of the largest impact
220 structures. A similar pattern is found when performing crater counts using craters as small as 250
221 m in diameter in a smaller subregion shown in Figure 3c. In this example, the four largest impact
222 craters with diameters of about 3 km (indicated by black arrows) affect the ages given by the crater
223 counts using smaller craters. The limited variations of crater densities and the spatial association
224 of lower crater densities with large impact craters indicates that the resurfacing processes affecting
225 the small impact crater population is dominated by impact cratering itself.

226 Periglacial features such as concentric crater fill can, nevertheless, be observed within
227 some large impact craters located in the northern region of the study area (i.e., crater numbers 11,
228 28 and 29 on Fig. 3b and Appendix A). These regions correspond to where the crater density
229 decreases independently of the presence of large impact craters (confer with the northeastern edge
230 of the study area). The reduced crater densities in these regions could be due to the intrinsic

231 variability of the small crater population, but could also be due to resurfacing processes or a bias
 232 resulting from lateral variations in target properties. The deconvolution of the influence of these
 233 three potential effects on the reduced crater densities obtained here (as well as on the ages of large
 234 impact craters located in this particular area) is deserving of a detailed local analysis that is beyond
 235 the scope of this study. We therefore do not exclude the possibility that resurfacing processes other
 236 than obliteration by impact cratering could play a local role affecting the shape of the crater SFD
 237 in this region. However, if other resurfacing processes operated in this region, the effect would
 238 preferentially decrease the crater density of the smallest impact craters. This bias can be mitigated
 239 by ensuring that the crater size-frequency distribution used to fit an isochron contains several
 240 diameter bins at the largest diameters.

241 **2.3 Large crater formation rate calculation**

242 In this section we describes how the ages of the layered ejecta deposits are determined, and
 243 how we determine the impact rate of large craters as a function of time from these measurements.
 244 Let's note D is the set of measured (small) impact craters. The likelihood function that the surface
 245 has a particular age t according to the set of observed craters D is given by Michael et al. (2016)
 246 in their Eq. (8):

$$247 \quad pr(D, t) \propto \exp\left(-A[C(d, t)]_{d_{min}}^{d_{max}}\right) (C(d = 1 \text{ km}, t))^{n_D}, \quad (1)$$

248 where A is the counting area, $C(d, t)$ is the cumulative form of the assumed production function
 249 that depends on crater diameter d and time t , d_{min} and d_{max} are the minimum and maximum crater
 250 diameters that are considered when evaluating the cumulative number of craters, and n_D is the total
 251 number of observed craters in the set D . Importantly, when the production function and counting
 252 area are known, the probability density function (pdf) depends only upon the minimum and

253 maximum crater diameters that are considered and the number of craters between these two limits.
 254 The technique allow to derive a model age probability, independent from the way whom the crater
 255 panel D is binned and also can provide a probability density function (pdf) for a surface with no
 256 impact craters.

257 The pdf associated with each layered ejecta crater dated in this study is calculated by
 258 following this formalism. Each individual pdf is then normalized to unit probability by integrating
 259 the distribution over time in steps of 1 Ma to assure that each crater has an equal influence on the
 260 final impact cratering rate calculation. The formation rate of large craters is then calculated as the
 261 sum of each normalized pdf, divided by the total surface area of the study region. For a given time
 262 interval, the sum of the normalized pdfs provides the expected number of impact craters that
 263 formed with sizes between d_{\min} and d_{\max} . For ease of comparison with other studies, we then
 264 convert our obtained impact rate for craters larger than 5 km in diameter to an impact rate for
 265 craters larger than 1 km using the equation

$$266 \quad \dot{n}(> 1km) = \frac{R}{A} \sum_{i=1}^N pdf_i \quad . \quad (2)$$

267 In this equation, \dot{n} is the impact rate per square km for craters larger than 1 km, R is the ratio
 268 between the number of craters larger than 1 km and 5 km accumulated on a surface of a given age
 269 (i.e. the study area age), A is the surface area of the study region, and N is the total number of
 270 craters dated.

271 We calculate the 1- σ uncertainty of the impact rate from the probability distribution
 272 functions of the individual craters using a Monte Carlo technique. Using the individual pdfs, we
 273 simulate a set of possible ages for each of the 53 impact craters in the study region. For each
 274 simulation, the cratering rate was calculated within bins of 250 Ma. Then, after performing one

275 thousand Monte Carlo simulations, the standard deviation of the cratering rate about the best fitting
276 value was computed.

277 **3. Is the inferred impact rate for large craters constant?**

278 The complete cratering record has been documented for craters with diameters larger than
279 5 km over the study area within Acidalia Planitia. All crater count results are given in Appendix
280 A, and the formation age of each large crater has been obtained using the method described in
281 section 2.1. Impact crater model ages vary from $0.05 \pm_{0.01}^{0.02}$ Ga to $2.20 \pm_{0.30}^{0.29}$ Ga (see Appendix
282 A). The model age of the study area is estimated to be $2.23 \pm_{0.10}^{0.10}$ Ga from the counting of all
283 craters larger than 500 m (see Appendix B).

284 Any dated craters have an age older than that of the study region. However, the probability
285 of some of the older craters to have an age older than that of the surface itself have a non-negligible
286 influence in the inferred impact rate calculated with the method described above. The variation of
287 the cratering density over the study area shown in Fig.3.b and the low uncertainty on its model age
288 suggest an emplacement occurred during a short period of time. The probability that a large crater
289 has an age older than that of the study region should be therefore close to 0. In order to limit this
290 calculation bias, we calculated the component of each pdf beyond the age of the study area and
291 redistributed them over the inferred impact rate, \dot{n} , between 0 and the age of the study area, 2.23
292 Ga. Nevertheless, this statistical redistribution only has a moderate effect on the inferred impact
293 rate results (see Appendix C). The overall interpretations of our results are therefore not affected
294 by this correction. All following discussion of the results is based on the inferred impact rate
295 corrected from the pdf component beyond the study region model age.

296 In Figure 4, the normalized age probability density functions for each of the large craters
297 are plotted using thin grey lines. The thick black curve in Fig. 4 represents the impact rate as a
298 function of time as determined by the ages of these craters, and the grey band about this curve
299 defines the 1- σ error on the impact rate. Finally, the red curve represents the value of the impact
300 rate over the last 3 Ga that is generally assumed being constant since ~ 2.5 Ga (Hartmann 2005).

301 As shown in Figure 4, the impact cratering rate is not constant between the present and
302 2.23 Ga when this region of Acidalia Planitia formed. In particular, the cratering rate for large
303 craters appears to be larger at younger ages than at older ages, with a difference of about a factor
304 of 3 between 500 Ma and 2 Ga. The total uncertainties in final model ages (including uncertainties
305 in counts) are estimated by Hartmann (2005) at \pm factor ~ 3 for this range of crater size. However,
306 we can assumed that the number of craters dated in this study should have statistically smoothed
307 the discrepancy between the inferred cratering rate and the Hartmann (2005) impact flux if the
308 chronology model used here was really constant. These results show that the cratering rate of large
309 craters is inconsistent with the assumed cratering rate of small craters.

310 We have processed all data using the chronologic system and production function of
311 Hartmann (2005). In order to test the sensitivity of our results to other chronological systems, as
312 described in Appendix D, we have reprocessed all our data using the systems of Hartmann and
313 Neukum (2001) and Ivanov (2001) (Appendix D). All these systems have an approximately
314 constant impact rate and a constant production function over the last 3 Ga. The application of other
315 chronological systems modifies the formation age obtained for each large crater and therefore the
316 inferred crater formation rate. However, none of the other models change the fact that the inferred
317 rate of formation of large impact craters varies with time in excess of the error bars. In particular,

318 the temporal variability of the computed impact cratering rate of large craters is roughly the same,
319 with the impact rate decreasing with increasing age.

320 **4 Discussion and conclusions**

321 The dating of a set of impact craters with layered ejecta on Acidalia Planitia has allowed
322 us to demonstrate that the cratering history for this region of Mars is inconsistent with a constant
323 rate of crater formation for both small and large craters (from 250 m to ~40 km) over the last ~2
324 Ga. This affect therefore the validity of the steep branch and the shallow branch of the crater PF
325 derived from power-law fits (Hartmann, 1999 , Hartmann and Neukum, 2001 , Hartmann, 2005).
326 This result implies that during this time, the production function must have varied. More
327 specifically, our results suggest that the impact flux of large craters was lower than predicted by
328 the assumed production function between about 1-2 Ga, and that the flux was larger than predicted
329 from about 1 Ga to 200 Ma. The inferred rate over the last 200 Ma is mainly dominated by a larger
330 crater formation rate than predicted. This observation is easiest to interpret in terms of temporal
331 changes in the production function, of which three hypothesis are possible. First, the impact flux
332 forming small craters could be constant with time, but that the formation rate of larger crater
333 increased with time over the past 2 Ga. Second, the flux of large impactors could alternatively be
334 constant with time, and that the impact rate of smaller craters decreased over time. Lastly, both the
335 small and large impactor flux could have varied with time with the relative flux of large craters
336 increasing over time.

337 A temporal variation in the production function would be directly connected to a temporal
338 variation of the size-frequency distribution of asteroids that cross the orbit of Mars. One possible
339 explanation for a change in the asteroid size-frequency distribution could be the disruption of one
340 or more asteroids (Culler et al, 2000, Nesvorny et al., 2002, 2005, Bottke et al., 2007, 2012, 2015).

341 In addition to affecting the asteroid SFD, the magnitude of the impact rate would likely be
342 increased for all diameters during a short period of time, typically a few tens of million years
343 (Bottke et al., 2007, 2015). Several studies have previously brought possible pieces of evidence
344 for temporal variations in the SFD of planet crossing asteroids, based both on lunar and terrestrial
345 data (Mazrouei et al., 2019 ; Bottke et al., 2002, 2015, 2016 ; Culler et al., 2000 ; Nesvorny et al.,
346 2002 ; Grier et al., 2001 ; Levine et al., 2005 ; Schmitz et al., 2016).

347 Dynamical evolution studies of the near-Earth object population (Bottke et al, 2015),
348 coupled to the SFD measured on several areas exhibiting different cratering densities / ages on the
349 Moon (McEwen et al., 1997; Ivanov et al., 2002) suggest that a deviation from a steady-state to a
350 factor 2 or so of large impactors SFD (>1km) during a long period of time should be modest since
351 ~3 Ga. Nevertheless, Mazrouei et al., 2019 suggest a decoupled formation rate between small and
352 large craters with the former constant and latter increasing at ~290 Ma due to asteroid break-ups
353 deduced from the model age of lunar craters younger than 1 Ga and larger than 10 km. This period
354 correspond roughly to the maximum of the inferred impact cratering rate measured in the present
355 study (Fig. 4). Their conclusion is consistent with our observation highlighting a decoupling in the
356 production function of small and large impact craters on Mars. The apparent increasing of the
357 inferred impact rate for large impact craters measured in our study could therefore be the result of
358 successive asteroid break-ups over the last 2 Ga. Among asteroid break-ups occurred in the
359 asteroid main belt, those having produced the Flora and Baptistina asteroid families, respectively
360 470 Ma ago (Nesvorny, et al. 2002, 2007, Durda, et al., 2007, Vokrouhlický, 2017) and 160 Ma
361 ago (Bottke et al, 2007), played a major role in providing impacts in the late history of the inner
362 Solar System. If some evidence of their influence on the impact cratering rate have been already

363 demonstrated on Earth and on the Moon, this is the first time that a potential signal from these
364 catastrophic events is observed on Mars.

365 Our results further challenge not only the hypothesis of a steady-state size distributions for
366 collisional population in the main belt (O'Brien and Greenberg, 2003) but also the hypothesis of a
367 constant impact flux and constant PF over the last 2 Ga within the inner Solar System (Hartmann,
368 2005 ; Hartmann and Neukum, 2001). Further work may attempt to decipher the evolution of the
369 PF with time using various sources of information, including *in-situ* dating of planetary materials
370 or radiometric ages of lunar and martian samples obtained from future sample return programs.
371 The crater counts produced by this study could be used for testing future chronological systems
372 involving time-dependent production function.

373

374 **Acknowledgments**

375 The authors would like to thank Mikhail Kreslavsky and Caleb Fassett for their detailed
376 and constructive reviews that improved the quality of our work. G.G. Michael provided helpful
377 suggestions concerning our observations. This research was funded by the GEOPS laboratory, the
378 Domaine d'Intérêt Majeur pour l'Astrophysique et les Conditions d'Apparition de la Vie (DIM
379 ACAV), the Programme National de Planétologie (PNP) of the Institut National des Sciences de
380 l'Univers (CNRS-INSU), the Centre National d'Etudes Spatiales (CNES), the Australian Research
381 Council (FT170100024) and by Curtin University (Perth, Western Australia, Australia).

382

383 **References**

- 384 Baratoux, D. et al. Mineralogical structure of the subsurface of Syrtis Major from OMEGA
385 observations of lobate ejecta blankets. *J. Geophys. Res.* 112, E08S05 (2007).
- 386 Barlow, N. et al. Standardizing the nomenclature of Martian impact crater ejecta morphologies. *J.*
387 *Geophys. Res.* 105, 26733-26738 (2000).
- 388 Bottke, W. F. et al. Dynamical evolution of main belt meteoroids: Numerical simulations
389 incorporating planetary perturbations and Yarkovsky thermal forces. *Icarus* 145, 301-331
390 (2000).
- 391 Bottke, W. F. et al. An asteroid breakup 160 Ma ago as the probable source of the K/T impactor.
392 *Nature* 449, 06070 (2007).
- 393 Bottke, W.F. et al. The collisional evolution of the main asteroid belt. In *Asteroids IV* (Michel, P.
394 et al., eds.), pp. 701–724. Univ. of Arizona, Tucson (2015).
- 395 Bottke, W.F. et al. On asteroid impacts crater scaling laws and a proposed younger surface age.
396 47th LPSC #2036 (2016).
- 397 Carr, M. and Head, J. Geologic history of Mars. *Earth and Planet. Sci. Lett.* 294, 185-203 (2010).
- 398 Christensen, P.R. et al. The Thermal Emission Imaging System (THEMIS) for the Mars 2001
399 *Odyssey Mission. Space Science Reviews*, 110, 85-130 (2004).
- 400 Culler, T. et al. Lunar impact history from $^{40}\text{Ar}/^{39}\text{Ar}$ dating of glass spherules. *Science* 287, 1785-
401 1788 (2000).
- 402 Dundas, C. et al. Role of material properties in the cratering record of young platy-ridged lava on
403 Mars, *Geophys. Res. Lett.*, 37, L12203, doi:10.1029/2010GL042869.
- 404 Durda, D. D. et al. Size–frequency distributions of fragments from SPH/N-body simulations of
405 asteroid impacts: Comparison with observed asteroid families. *Icarus* 186, 498–516 (2007).

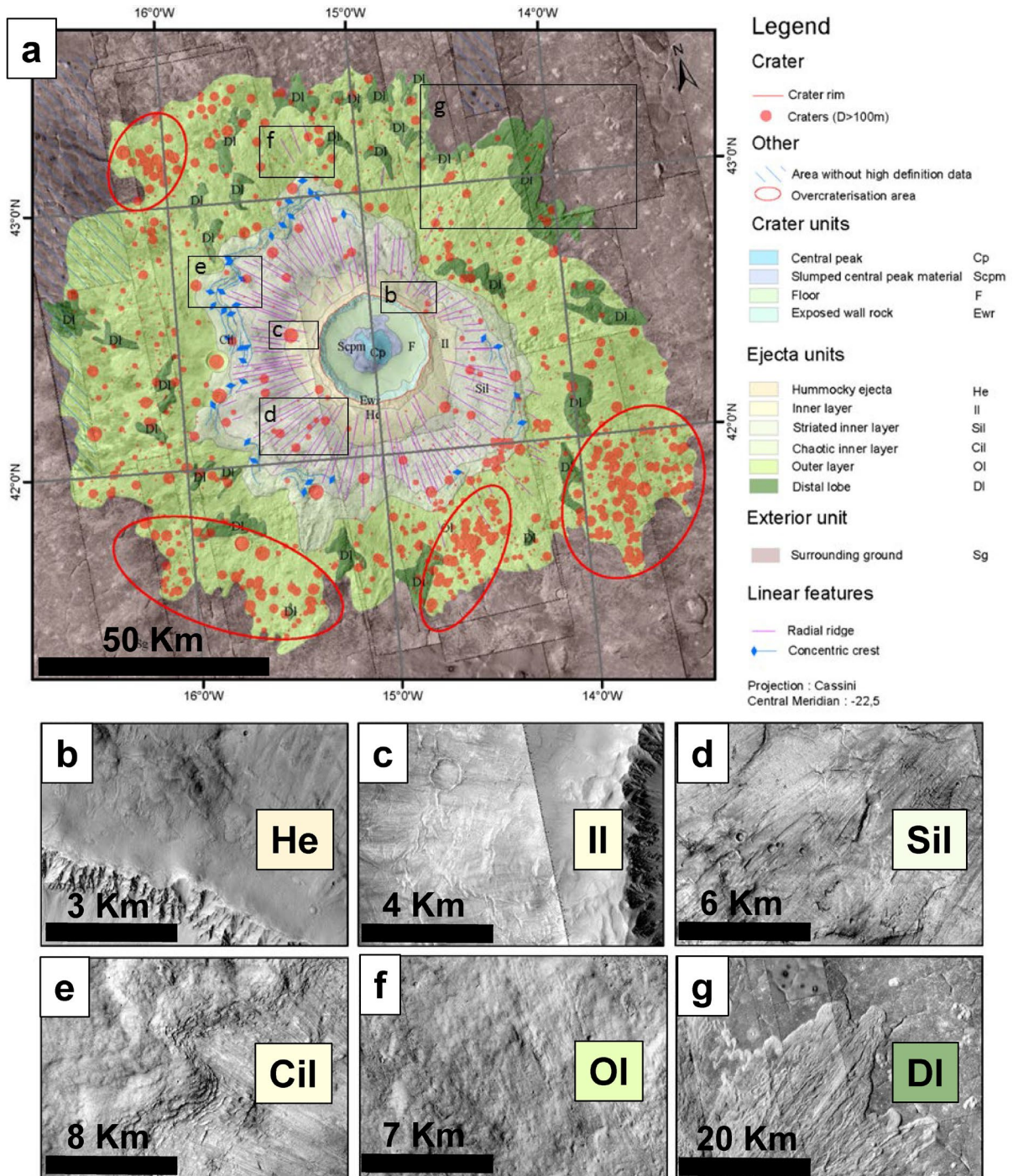
- 406 Grier, J. A. et al. Optical maturity of ejecta from large rayed lunar craters. *J. Geophys. Res.* 106,
407 32847-32862 (2001).
- 408 Hartmann, W.K. Martian cratering 6: Crater count isochrons and evidence for recent volcanism
409 from Mars Global Surveyor. *Meteoritics and Planetary Science*, 34, 167-177 (1999).
- 410 Hartmann, W.K. and Neukum, G.G. Cratering chronology and the evolution of Mars. *Sp. Sci.*
411 *Reviews.* 96, 165-194 (2001).
- 412 Hartmann, W. K. Martian cratering 8: Isochron refinement and the chronology of Mars. *Icarus*
413 174, 294-320 (2005).
- 414 Hartmann, W.K. et al., Do young martian ray craters have ages consistent with the crater count
415 system? *Icarus* 208, 621-635 (2010).
- 416 Ivanov, B. Mars Moon cratering rate ratio estimates. *Chronology and evolution of Mars.* 96, 87-
417 104 (2001).
- 418 Ivanov, B. A. et al., The comparison of size-frequency distributions of impact craters and asteroids
419 and the planetary cratering rate. In *Asteroids III* (W. F. Bottke Jr. et al., eds.), pp. 90–101.
420 Univ. of Arizona, Tucson. (2002).
- 421 Kadish, S. and Head, J. The ages of pedestal craters on Mars: Evidence for a late-Amazonian
422 extended period of episodic emplacement of decameters-thick mid-latitude ice deposits.
423 *Planet. Space Sci.* 91, 91-100 (2014).
- 424 Kirchoff, M.R., et al. The effects of terrain properties on determining crater model ages of lunar
425 surfaces. 46th LPSC #2121 (2015).
- 426 Kneissl, T. et al. Map-projection-independent crater size-frequency determination in GIS
427 environments: New software tool for ArcGIS. *Planet. Space Sci.* 59, 1243-1254 (2011).

- 428 Kreslavsky, M. and Head III, J. Mars: Nature and evolution of young latitude-dependent water-
429 ice-rich mantle. *GRL*, 14 (2002).
- 430 Kreslavsky, M. and Head III, J. North–south topographic slope asymmetry on Mars: Evidence for
431 insolation-related erosion at high obliquity. *GRL*, 30 (2003).
- 432 Kreslavsky, M. and Head III, J. Mars Climate History: Insights From Impact Crater Wall Slope
433 Statistics. *GRL*, 45 (2018).
- 434 Lagain, A. et al., Datation of Multiple-Layer ejecta crater on Mars. 46th Lunar and Planetary
435 Science Conference Abstract #1920 (2015).
- 436 Le Feuvre, M. and Wieczorek, M. A. Non-uniform cratering of the Moon and a revised crater
437 chronology of the inner solar system. *Icarus* 214, 1-20 (2011).
- 438 Levine, J. et al. $^{40}\text{Ar}/^{39}\text{Ar}$ dating of Apollo 12 impact spherules. *Geophys. Res. Lett.* 32, L15201
439 (2005).
- 440 Mazrouei, S. et al. Earth and Moon impact flux increased at the end of the Paleozoic. *Science*
441 6424, 253-257 (2019).
- 442 McEwen A. S. et al. The phanerozoic impact cratering rate: Evidence from the far side of the Moon.
443 *Journal of Geophysical Research*, 102, 9231–9242. (1997).
- 444 Michael, G. G. and Neukum, G. Planetary surface dating from crater size frequency distribution
445 measurements: Partial resurfacing events and statistical age uncertainty. *Earth Pl. Sci. Lett.*
446 294, 223-229 (2010)
- 447 Michael, G. G. et al. Planetary surface dating from crater size frequency distribution
448 measurements: spatial randomness and clustering. *Icarus* 218, 169-177 (2012).
- 449 Michael, G. G. et al. Planetary surface dating from crater size-frequency distribution
450 measurements: Poisson timing analysis. *Icarus* 277, 279-285 (2016).

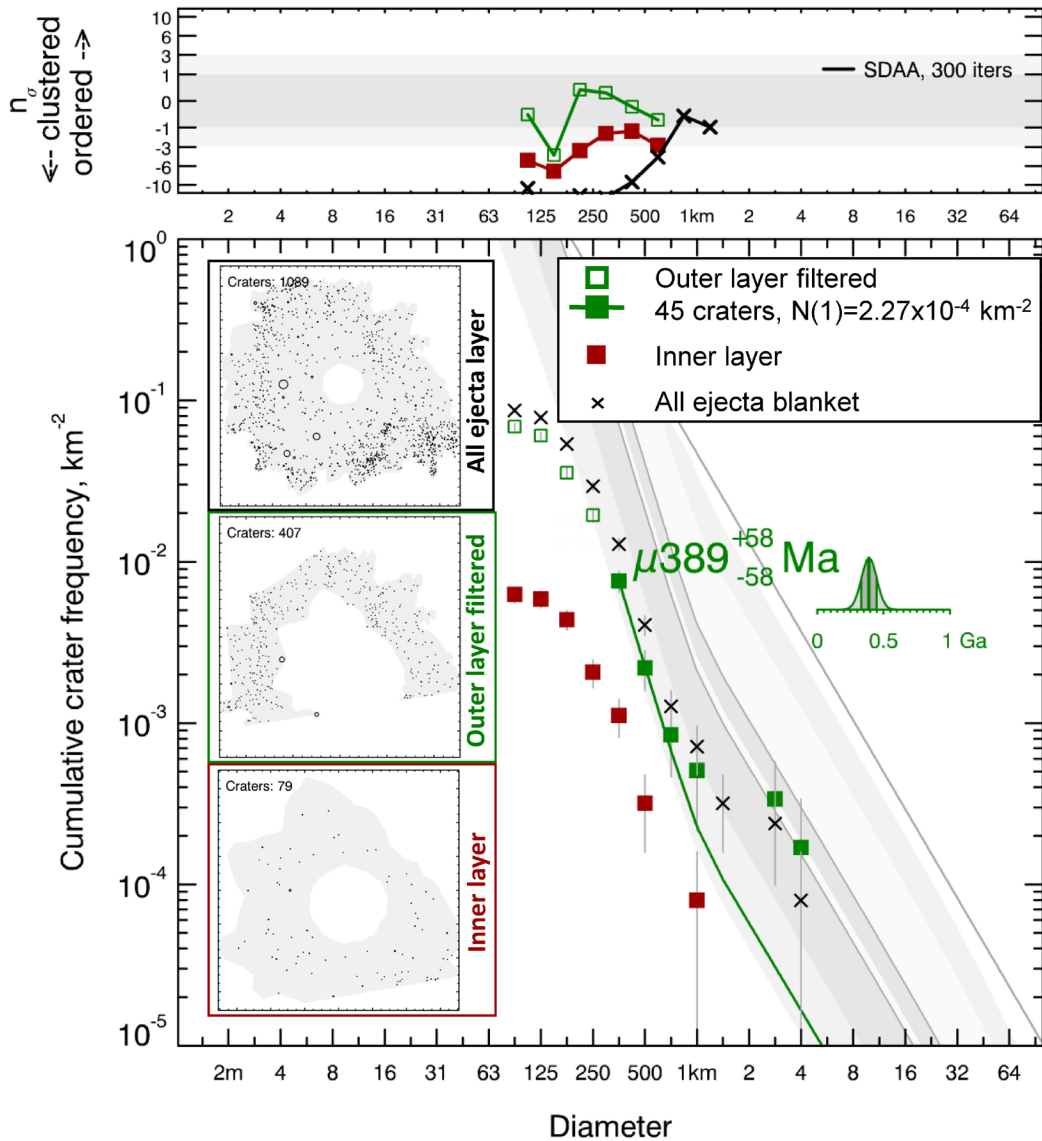
- 451 Nesvorny, D. et al. The Flora family: a case of the dynamically dispersed collisional swarm? *Icarus*
452 157, 155-172 (2002).
- 453 Nesvorny, D. et al. Evidence for asteroid space weathering from the Sloan Digital Sky Survey.
454 *Icarus* 173, 132–152. (2005).
- 455 Nesvorny, D. et al. Express delivery of fossil meteorites from the inner asteroid belt to Sweden.
456 *Icarus* 188, 400–413 (2007).
- 457 Neukum, G. et al. Cratering record in the inner Solar System in relation to the lunar reference
458 system. *Space Science Review* 96, 55-86 (2001).
- 459 O'Brien, D.P. and Greenberg, R. Steady-state size distributions for collisional populations:
460 Analytical solution with size dependent strength. *Icarus* 164, 334-345 (2003).
- 461 Platz, T. et al. Crater-based dating of geological units on Mars: Methods and application for the
462 new global geological map. *Icarus*, 225, 806-827 (2013).
- 463 Quantin, C. et al. Possible long-term decline in impact rates: 1. Martian geological data. *Icarus*
464 186, 1-10 (2007).
- 465 Quantin, C. et al. The Lunar cratering rate over the last 1 Gy inferred from the age of the lunar ray
466 craters. 46th Lunar and Pl. Sci. Conf. Abstract #2692 (2015).
- 467 Robbins, S. and Hynek, B. A new global database of Mars impact craters ≥ 1 km: 1. Database
468 creation, properties, and parameters. *JGR*, 117, E5 (2012).
- 469 Schmitz, B. et al. A new type of Solar-System material recovered from Ordovician marine
470 limestone. *Nature* 7, 11851 (2016).
- 471 Schon, S.C. et al. Recent high-latitude resurfacing by a climate-related latitude-dependant mantle:
472 Constraining age of emplacement from counts of small craters. *Pl. Sp. Sci.* 69, 49-61 (2012).

- 473 Stöffler, D. et al. Cratering history and lunar chronology. *Rev. Mineral Geochem.* 60, 519–596
474 (2006).
- 475 Tanaka, K. et al. *Geologic map of Mars*. USGS (2014).
- 476 Tikoo, S.M. et al. A two-billion-year history for the lunar dynamo. *Science Advances* 3, 8 (2017).
- 477 Vokrouhlický, D. et al. Forming the Flora Family: Implications for the Near-Earth Asteroid
478 Population and Large Terrestrial Planet Impactors. *The Astronomical Journal* 153:172 (23pp)
479 (2017).
- 480 Weiss, D.K. and Head, J. Formation of double-layered ejecta craters on Mars: A glacial substrate
481 model. *Geoph. Res. Lett.* 40, 3819-3824 (2013).
- 482 Werner, S.C.. The early martian evolution – Constraints from basin ages. *Icarus*, 195, 45-60
483 (2008).
- 484 Wulf, G. and Kenkmann, T. A high-resolution study of Double-layered ejecta craters: morphology,
485 inherent structure, and phenomenological modeling. *Meteorit. Planet. Sci.* 50, 173-203
486 (2015).
- 487 Zanetti, M. et al. Evidence for self-secondary cratering of Copernican-age continuous ejecta
488 deposits on the Moon. *Icarus* 298, 64-77 (2017).
- 489 Zellner, N.E.B. and Delano, J.W. $^{40}\text{Ar}/^{39}\text{Ar}$ ages of lunar impact glasses: Relationships among Ar
490 diffusivity, chemical composition, shape, and size. *Geochimica et Cosmochimica Acta* 161, 203-
491 218 (2015).

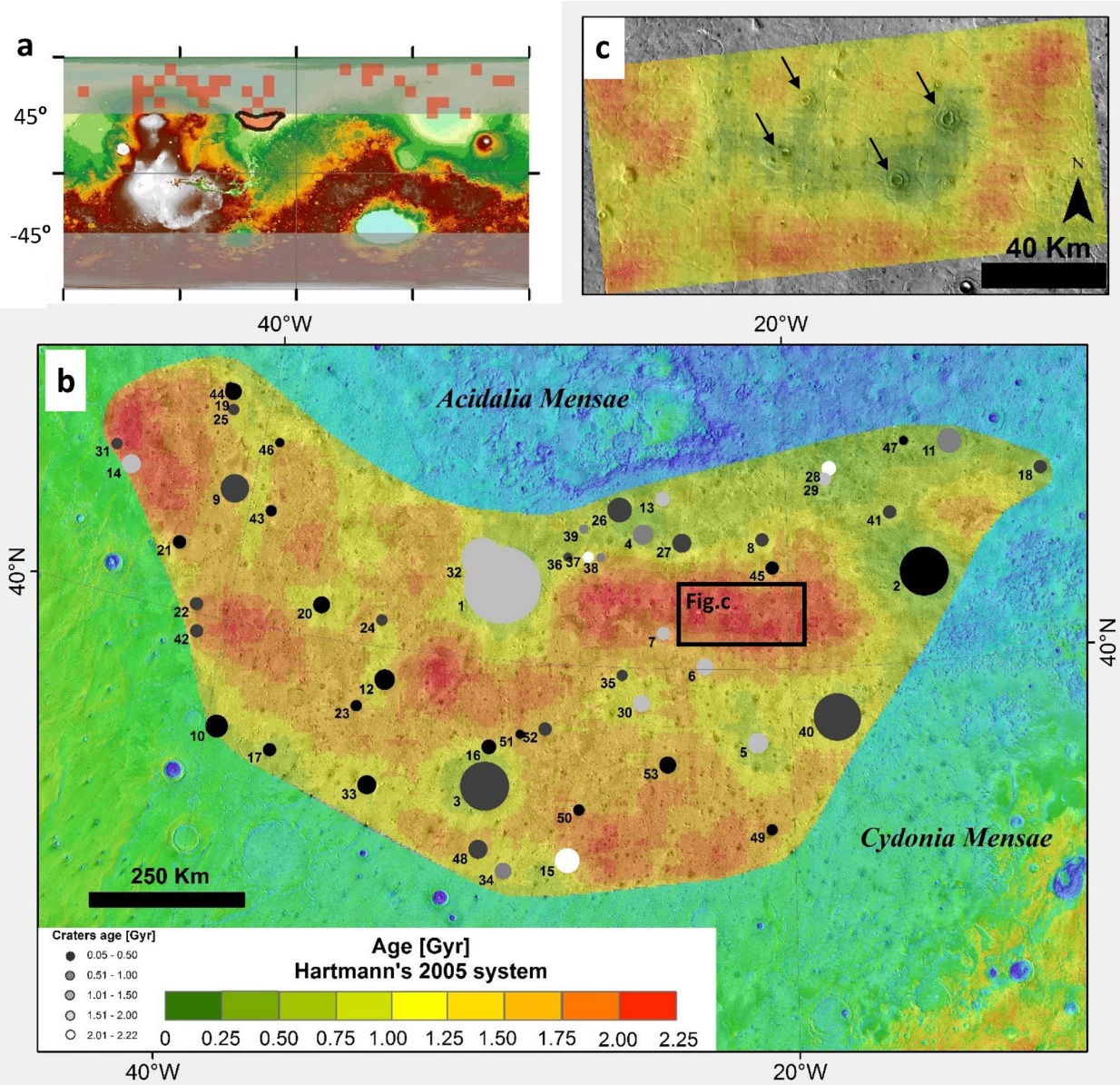
1 **Figures**



2
3 **Figure 1: a:** Geological map of the Arandas impact crater. Craters larger than 100 meter
4 identified on its ejecta blankets (n=1095) are marked with red dots. Four “overcratered” areas are
5 noted with red ellipses. **b-g:** Close-up showing respectively the He, Il, Sil, Cil, Ol and Dl units.



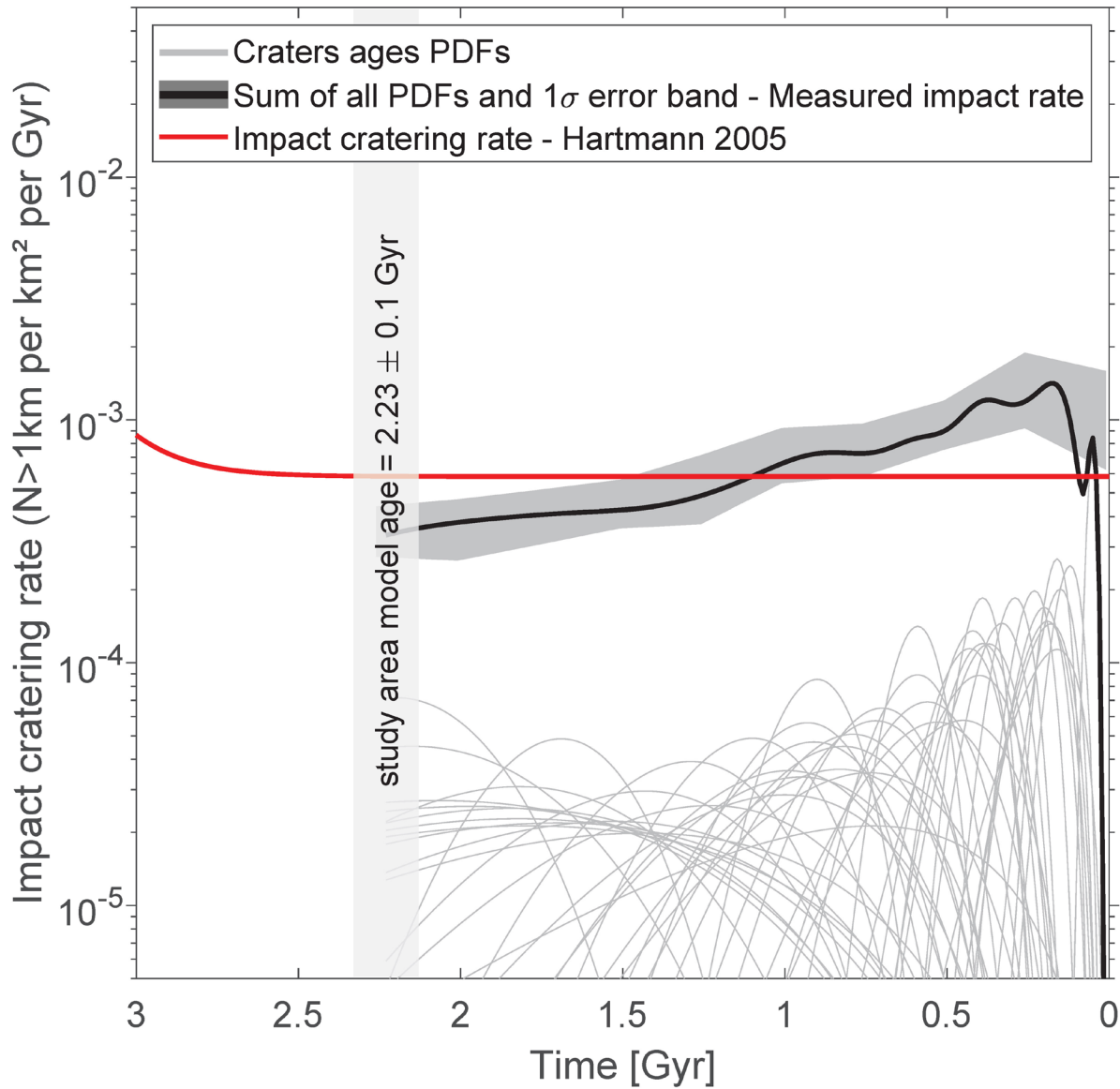
6
 7 **Figure 2:** CSFDs extracted from three areas on the ejecta blanket of the Arandas impact crater: in
 8 red, the inner layer, in green, the outer layer without overcratered regions and in black the entire
 9 surface of ejecta layer. Top: Results of the Randomness Analysis (Michael, et al., 2012) performed
 10 on each of three CSFDs. Bottom: Incremental representation of the three CSFDs and associated
 11 isochrones fitted with Hartmann's (2005) chronology system (Michael et al., 2010, 2016). The
 12 northern part of the outer layer (in green) contained the most spatially randomly distributed
 13 population of craters among these three areas. A fit from this CSFD has therefore been applied and
 14 an age of $\mu 389 \pm_{58}^{58}$ Myr has been retained for the emplacement of Arandas crater.



15

16 **Figure 3:** Study area selection. (a) Map showing areas with more than 80% of craters larger than
 17 5 km associated with continuous ejecta blankets (Robbins et al. 2012, Lagain et al., 2019,
 18 submitted) (red squares). The area highlighted by a black contour is the only region that satisfies
 19 the two selection criteria described in the text. (b) Map of the model age variability of Acidalia
 20 Planitia from the crater density map for craters larger than 500 m. Each crater > 5 km in diameter
 21 is represented by a filled circle. The size of the circle is proportional to its diameter, the grey shade
 22 corresponds to the crater age, and the number corresponds to its ID number in Appendix A. We

23 observe that the crater density and model age is generally lower around the largest craters ($D > \sim$
24 10 km). **(c)** Close-up of the study area where the crater density ($D > 500$ m) is the highest. Here,
25 model ages are derived from craters larger than 250 m, and we also observe lower crater densities
26 around largest impact craters (black arrows) that are about 3 km in diameter. Model ages map
27 displayed on sub-figures b and c are sharing the same color.



28

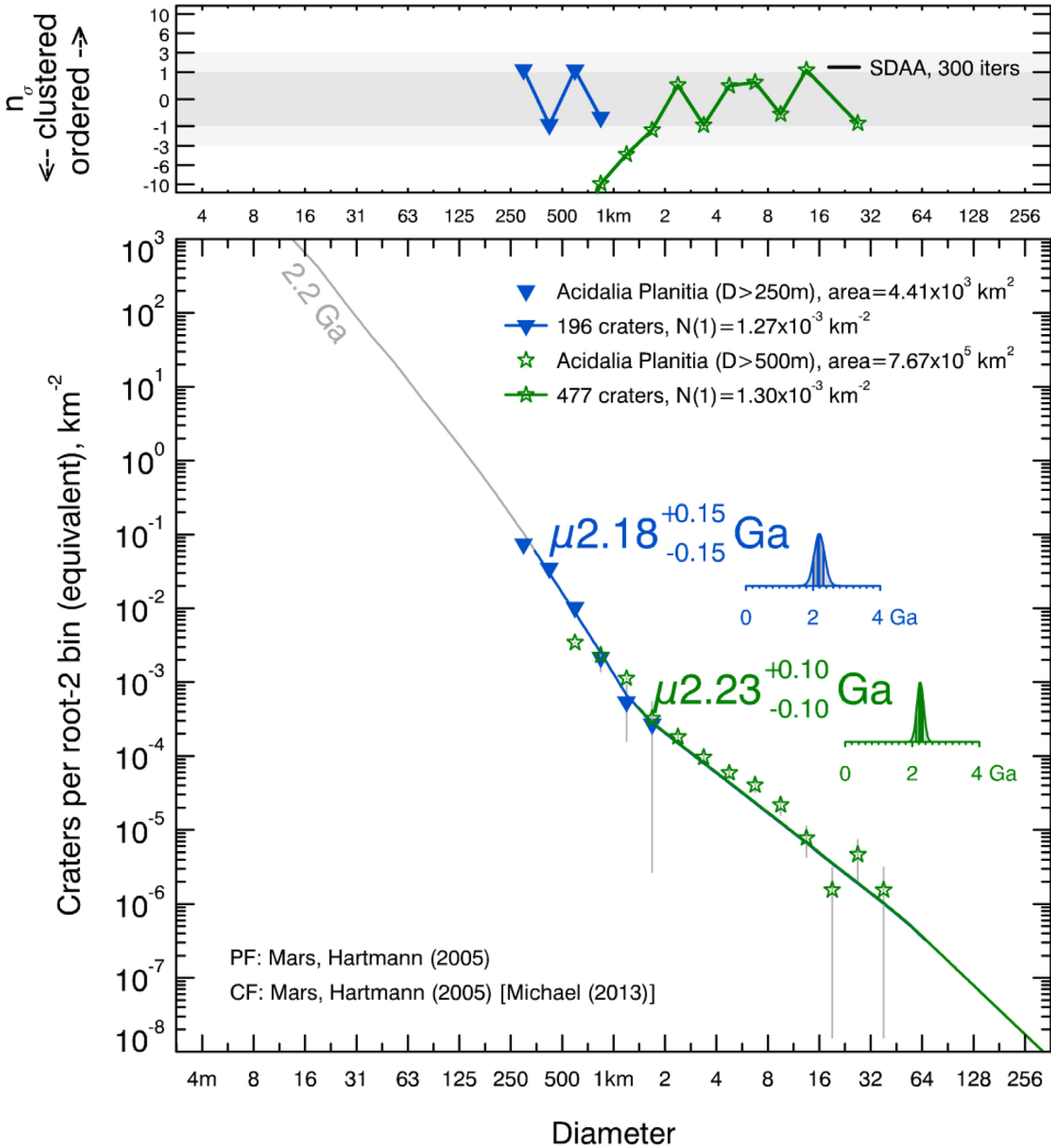
29 **Figure 4:** Model ages probability density function of each crater (grey curves) in the Acidalia
 30 Planitia study region and the inferred rate of formation of these craters (black curve). The grey band
 31 correspond to its 1 sigma error calculated by step of 250 Myr. The Hartmann (2005) impact
 32 cratering rate is displayed as a red curve (constant for the last 2.5 Gyr).

1 **Appendix A. Absolute ages and other statistical parameters of the CSFD statistics measured**
 2 **for the ejecta blankets of craters shown in Fig.3.**

ID	Latitude [°]	Longitude [°]	Diameter [km]	Counting Area [km ²]	Number of craters counted	Number of craters fitted	Range of diameters used to fit (min - $\sqrt{\text{Area}}$)	Model age [Gyr] Hartmann, 2005	Error [Gyr]
1	42.02	-30.41	40.4	5730	273	56	500m - 76km	μ 1.69	+0.22 -0.22
2	42.42	-15.01	24.4	9010	407	45	354m - 77km	μ 0.39	+0.06 -0.06
3	36.56	-30.41	26.7	3170	133	16	500m - 56km	μ 0.91	+0.24 -0.20
4	43.63	-25.36	11.1	1220	123	8	500m - 35km	μ 1.23	+0.46 -0.37
5	38	-21.19	10	557	55	6	500m - 24km	μ 1.97	+0.69 -0.63
6	40.06	-23.02	7.8	425	54	4	500m - 21km	μ 1.79	+0.78 -0.67
7	40.95	-24.51	7	561	74	5	500m - 24km	μ 1.70	+0.72 -0.60
8	43.51	-20.93	8	613	90	24	250m - 25km	μ 0.59	+0.12 -0.12
9	43.44	-40.67	14.6	1110	48	15	354m - 33km	μ 0.72	+0.20 -0.17
10	37.19	-39.65	11.7	494	20	16	177m - 22km	μ 0.16	+0.04 -0.04
11	45.87	-13.59	13.4	899	87	22	354m - 30km	μ 1.29	+0.29 -0.25
12	39.13	-34.19	10.8	926	45	20	250m - 30km	μ 0.33	+0.08 -0.07
13	44.6	-24.66	7.6	514	53	5	500m - 23km	μ 1.82	+0.73 -0.64
14	43.39	-44.62	10.1	700	29	7	500m - 26km	μ 1.84	+0.66 -0.57
15	34.69	-27.5	13.1	1720	251	6	707m - 41km	μ 2.07	+0.68 -0.66
16	37.63	-30.37	7	313	66	28	177m - 18km	μ 0.42	+0.08 -0.08
17	36.82	-37.75	7.1	749	31	17	250m - 27km	μ 0.37	+0.09 -0.08
18	44.84	-10.25	7.1	1370	93	18	354m - 37km	μ 0.70	+0.17 -0.15
19	45.92	-41.54	8.4	393	16	13	125m - 20km	μ 0.05	+0.02 -0.01
20	40.86	-36.77	8.4	1280	25	25	250m - 36km	μ 0.29	+0.06 -0.06
21	41.73	-42.21	7.9	332	18	8	177m - 18km	μ 0.12	+0.05 -0.04
22	40.24	-41.14	6.5	531	41	8	354m - 23km	μ 0.83	+0.31 -0.25
23	38.33	-35.05	6.5	186	12	7	177m - 14km	μ 0.19	+0.08 -0.06
24	40.7	-34.56	6.4	459	32	6	354m - 21km	μ 0.74	+0.32 -0.25
25	45.46	-41.37	6.2	257	19	2	354m - 16km	μ 0.73	+0.44

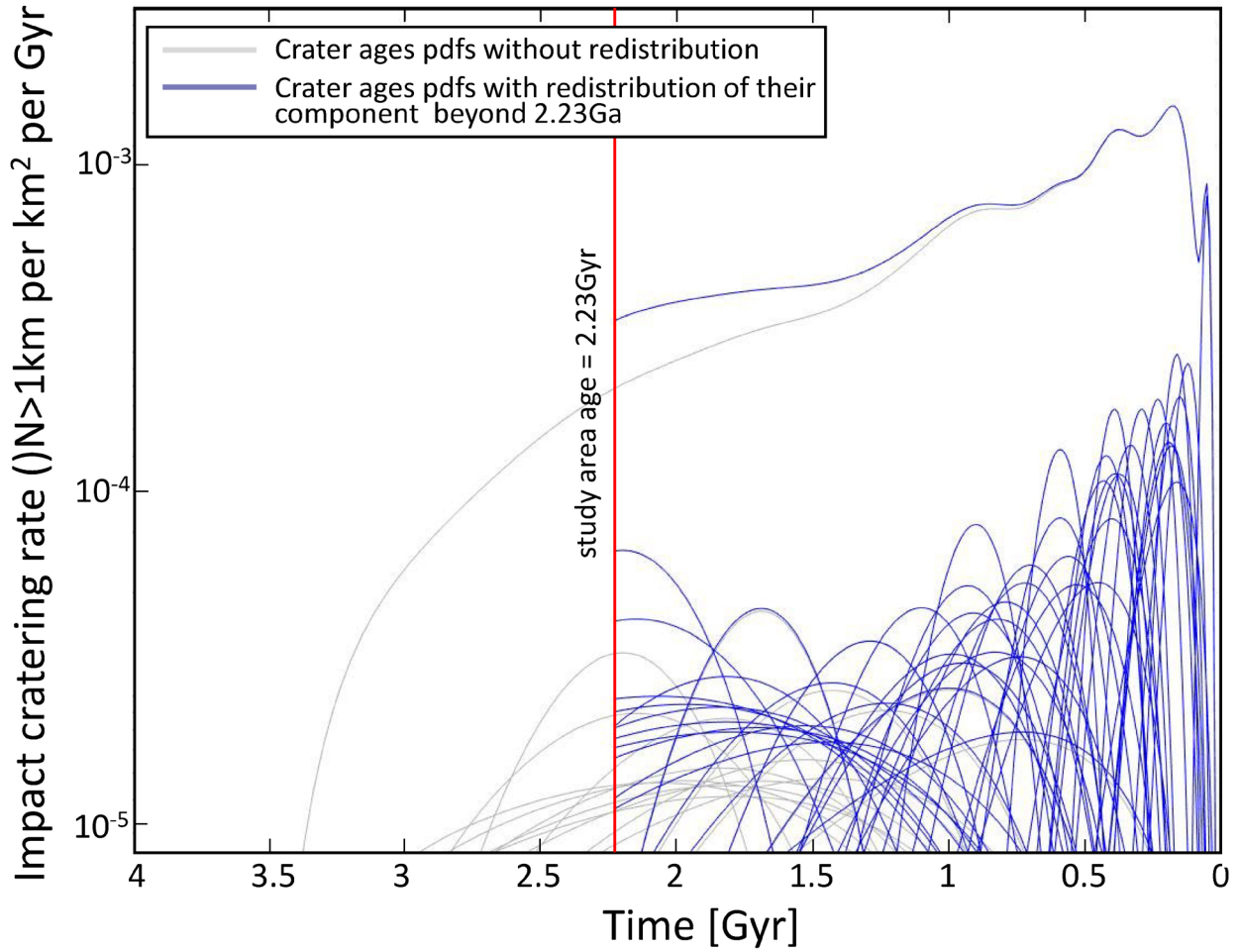
									-0.31
26	44.26	-26.27	12.4	1320	162	24	354m - 36km	μ 0.93	+0.19 -0.19
27	43.42	-23.9	10.6	1330	98	7	500m - 36km	μ 1.00	+0.40 -0.32
28	45.38	-18.3	7.3	508	64	21	354m - 23km	μ 2.15	+0.45 -0.42
29	45.09	-18.49	6.7	425	54	4	500m - 21km	μ 1.79	+0.78 -0.67
30	39.03	-25.21	8.3	220	31	6	354m - 15km	μ 1.53	+0.64 -0.51
31	43.78	-45.33	6.1	368	31	13	250m - 19km	μ 0.56	+0.16 -0.14
32	42.67	-31.22	21.6	1480	75	15	500m - 38km	μ 1.82	+0.48 -0.42
33	36.26	-34.35	9.2	747	41	21	250m - 27km	μ 0.43	+0.10 -0.09
34	34.31	-29.58	8.9	553	62	4	500m - 24km	μ 1.44	+0.72 -0.56
35	39.78	-25.92	5.4	244	33	8	250m - 16km	μ 0.53	+0.20 -0.16
36	42.91	-28.09	5.7	278	39	14	250m - 17km	μ 0.79	+0.22 -0.19
37	42.94	-27.35	5.9	360	93	53	250m - 19km	μ 2.20	+0.29 -0.30
38	42.95	-26.88	5.7	340	75	25	250m - 18km	μ 1.10	+0.22 -0.22
39	43.7	-27.56	5	153	35	14	250m - 12km	μ 1.43	+0.40 -0.34
40	38.63	-18.43	24.8	1520	186	60	250m - 39km	μ 0.59	+0.08 -0.08
41	44.09	-16.1	7	600	41	11	354m - 24km	μ 0.99	+0.32 -0.26
42	39.55	-40.94	6.9	521	37	9	354m - 23km	μ 0.95	+0.34 -0.27
43	43.06	-39.18	5.4	250	23	10	177m - 16km	μ 0.20	+0.07 -0.06
44	46.02	-41.7	5.1	186	13	7	177m - 14km	μ 0.19	+0.08 -0.06
45	42.74	-20.56	7.1	441	48	11	250m - 21km	μ 0.40	+0.13 -0.10
46	44.89	-39.38	5.1	173	12	6	177m - 13km	μ 0.18	+0.08 -0.06
47	44.97	-15.35	5	106	11	3	177m - 10km	μ 0.16	+0.10 -0.07
48	34.84	-30.47	9.8	3330	148	51	354m - 54km	μ 0.90	+0.13 -0.13
49	35.63	-20.76	6.6	754	86	19	250m - 27km	μ 0.39	+0.09 -0.08
50	36.09	-27.21	5.8	265	19	8	177m - 16km	μ 0.15	+0.06 -0.05
51	38.04	-29.35	5	222	22	6	250m - 15km	μ 0.45	+0.20 -0.15
52	38.23	-28.51	6.1	786	47	12	354m - 28km	μ 0.82	+0.25 -0.21
53	37.39	-24.27	8.7	379	46	18	177m - 19km	μ 0.23	+0.06 -0.05
study area	/	/	/	767 000	4909	477	1.41km - 875km	μ 2.23	+0.10 -0.10
				4410	453	196	354m - 66km	μ 2.18	+0.15 -0.15

3 **Appendix B. Study area dating from craters larger than 250m in diameter on the restricted**
 4 **area shown on Figure 3.c, blue isochron, and on the entire study area from craters larger**
 5 **than 500m in diameter (Figure 3.b), green isochron. The results of the Randomness Analysis**
 6 **performed for the two CSFDs is displayed at the top of the figure.**



7
 8
 9
 10
 11
 12

13 **Appendix C. Inferred impact cratering rate calculated from crater ages pdfs with and without**
 14 **a redistribution of their component beyond 2.23 Ga, respectively in blue and grey. Slight**
 15 **modifications brought from this correction affect preferentially the impact rate close to the**
 16 **age of the study region. The blue curve is the same as that shown in Fig.4.**



17
 18
 19
 20
 21
 22
 23
 24
 25
 26
 27
 28

29 **Appendix D. a: Constant impact rate proposed by Hartmann (2005), Hartmann & Neukum (2001) and Ivanov (2001). b: Chronology function linked to these three impact rates. c-e:**
 30 **Chronology function linked to these three impact rates. c-e: Comparison of the gap between the model and the inferred impact rate respectively deduced**
 31 **by Hartmann (2005), Hartmann & Neukum (2001) and Ivanov (2001).**
 32

